



## Research paper

# Experimental study of the effect of rock blasting with various cutting forms for tunnel excavation using physical model tests

H. An<sup>1</sup>, Y. Song<sup>2</sup>, D. Yang<sup>3</sup>

**Abstract:** Cutting blasting has been widely used for tunnel excavation. The cutting forms significantly influence the blasting effect. This research focuses on the study of the relationship between cutting forms and blasting effects. Similarity theory is proposed for the experimental study of the rock blasting using small models. Then four experimental modes with different cutting forms are used to study the blasting effect due to the cutting forms. The cutting depth, borehole utilization rate, fragments volume, and average fragment size are analysed. The blasting effects with various cutting forms are compared. The influences of the borehole space and the blasting delay are discussed. It is concluded that the spiral cutting form can produce more fragments and is recommend for the small section tunnel excavation.

**Keywords:** rock blasting, cutting blasting, rock fracture, cutting forms, physical model

<sup>1</sup> Lecturer, PhD., Eng., Kunming University of Science and Technology, Faculty of Public Security and Emergency Management, 650093, Kunming, China, e-mail: [huaming.an@yahoo.com](mailto:huaming.an@yahoo.com), ORCID: <https://orcid.org/0000-0003-2254-2276>

<sup>2</sup> ME., Eng., Eng., Kunming University of Science and Technology, Faculty of Public Security and Emergency Management, 650093, Kunming, China, e-mail, [yushan.song@stu.kust.edu.cn](mailto:yushan.song@stu.kust.edu.cn), ORCID: <https://orcid.org/0000-0002-6435-863X>

<sup>3</sup> PhD., Eng., University of Science and Technology Beijing, School of Civil and Resource Engineering, 100083, Beijing, China, e-mail: [zydqyang@163.com](mailto:zydqyang@163.com)

## 1. Introduction

The rapid development of modern society has resulted in need for increased underground engineering, such as mining, tunnels, and dams. Rock blasting is one of the main technology frequently used for underground excavation, which is used in many civil engineering, e.g. hard rock tunnelling and structure demolition [1]. For engineering applications, many empirical models or equations have proposed and implemented in engineering projects [2–4]. Besides, many experimental studies have been used to describe the rock fracture process during rock blasting and develop the fracture mechanism [5–8]. Additionally, many numerical methods have been developed for modelling the rock blasting process due to the rapid development of computational technologies, e.g. ANSYS-LSDYNA [9], ABAQUS [10, 11], LS-DYNA [12–14] and AUTOYN [15].

As cutting blasting is one of the blasting technology widely used as the first step for underground excavation, this researches focus on the study of cutting blasting using experimental methods. The cutting methods can be clarified as oblique-hole cutting blasting and straight-hole cutting blasting. For the small and medium cross-section tunnel excavation, the straight-hole cutting blasting method is the most economical and practical. Many studies have been done for optimizing blasting technologies. Huang, Qiu et al. (2019) carried out the research for reducing the vibration induced by cutting blasting [16]. According to their studies, it is concluded that longer delay intervals of rock blasting can reduce the peak particle velocity [16]. Liu, Li et al. (2018) studied the one-step raise excavation technology by experimental and numerical methods [17]. Man, Liu et al. (2018) designed the blasting parameters for cutting blasting explosion in a tunnel and compared the blasting effects of three different cutting methods [18]. Xie, Lu et al. (2017) focused their study on the influence of the in situ stress on the blasting effect for cutting blasting [19]. Xie, Lu et al. (2016) used the LS-DYNA to study cutting blasting subjected to high in-situ stress [20]. Qu, Zheng et al. (2008) also carried out numerical study for cutting blasting using ANSYS/LS-DYNA 3D nonlinear dynamic finite element software, and they found that the uncharged borehole played important role in the rock blasting process [21].

Although many studies have been carried out for optimizing the cutting blasting technology, it is still far from a better understanding of rock mechanism during cutting blasting. In addition, it is hard to design the cutting forms for certain tunnels if considering the blasting effect and economic demand. Thus, in this search, cutting forms are studied by small scale on the basis of the similarity theory.

## 2. Similarity analysis and similarity model

As experimental tests in the underground excavation is time and money consuming, this research is carried out by the physical model tests, i.e. small scale test, based on the similarity theory. In order to establish the physical model, the parameters for the physical model should be studied first on the basis of the similarity theory, which includes geometric parameters, explosive performance parameters, rock performance parameters and time parameters. Among them, the geometric parameters consist of minimum resistance line, depth boreholes, borehole radius, charge radius, the spacing of borehole row, spacing between boreholes in the same row. The explosive parameters include the density of explosives, detonation velocity of explosives, and unit consumption of explosives. Rock parameters include rock density, rock strength, rock wave impedance and rock elastic modulus; time parameter is the delay time.

In this paper, the cutting depth, rock fragment volume and blasting fragmentation are taken as the main indexes to evaluate the blasting effect for cutting blasting.

### 2.1. Similarity criterion

Shan, Huang et al. (2012) proposed a similarity criterion for modelling cutting blasting using physical model tests and focuses their study on the cutting blasting modelling test [22]. The similarity criterion is established in this research on the basis of those well documented physical models in the literature [22]. The basic dimensions in force system, i.e. length dimension L, time dimension T and force dimension F, is used to describe the parameters in rock blasting. Table 1 illustrates the parameter and its dimension and all the parameters used in this section can be found in the Table 1. It should be noted that the time delay for rock blasting is not considered in the following table. It is supposed that the time delay is the same between the physical model test and actual rock blasting underground.

According to the similarity theory, the main parameters can be expressed as follows.

$$(2.1) \quad f(H, V, D, w_d, h, r_b, r_c, a, b, \rho_c, v, q, \rho_r, \sigma, \rho_o, c, E) = 0$$

All the parameters can be expressed by the basic dimensions, e.g.  $w_d$ ,  $\rho_c$ , and  $v$ , as illustrated in the following equations.

$$(2.2) \quad \begin{aligned} \pi_1 &= \frac{H}{w_d}, & \pi_2 &= \frac{V}{w_d^3}, & \pi_3 &= \frac{D}{w_d}, & \pi_4 &= \frac{h}{w_d}, & \pi_5 &= \frac{r_b}{w_d}, & \pi_6 &= \frac{r_c}{w_d}, & \pi_7 &= \frac{a}{w_d}, \\ \pi_8 &= \frac{b}{w_d}, & \pi_9 &= \frac{q}{\rho_c}, & \pi_{10} &= \frac{\rho_r}{\rho_c}, & \pi_{11} &= \frac{\sigma}{\rho_c v^2}, & \pi_{12} &= \frac{\rho_o c}{\rho_c v}, & \pi_{13} &= \frac{E}{\rho_c v^2}. \end{aligned}$$

When the geometric parameters ( $w_d$ ,  $h$ ,  $r_b$ ,  $r_c$ ,  $a$ ,  $b$ ), explosive performance parameters ( $\rho_c v$ ), rock performance parameters ( $\rho_r$ ,  $\sigma$ ,  $\rho_r c$ ,  $E$ ) and explosive unit consumption ( $q$ ) are known, the  $H$ ,  $V$  and  $D$  can be calculated according to the rock blasting design. Thus, similarity criterions can be expressed as follows

$$(2.3) \quad \pi_1, \pi_2, \pi_3 = f(\pi_4, \pi_5, \pi_6, \pi_7, \pi_8, \pi_9, \pi_{10}, \pi_{11}, \pi_{12}, \pi_{13})$$

It can be seen that there are 10 main factors that affect the cutting depth, blasting volume and blasting fragmentation in tunnel excavation blasting. Among them,  $\pi_4$ ,  $\pi_5$ ,  $\pi_6$ ,  $\pi_7$ ,  $\pi_8$ , are the basis for selecting model size, while  $\pi_9$ ,  $\pi_{10}$ ,  $\pi_{11}$ ,  $\pi_{12}$ ,  $\pi_{13}$  are the basis for choosing similar materials and explosives.

Therefore, in order to make the model test results reflect the field blasting situation, the three groups of parameters should be determined before the test.

## 2.2. Physical model tests and similarity constant

According to the similarity criterion for straight-hole cutting blasting in tunnel excavation, the similarity of the model test can be attributed to the geometric similarity, material similarity and blasting dynamic similarity of the model. Therefore, the geometric similarity constant, material similarity constant and blasting dynamic similarity constant should be determined before the model test.

For the cutting blasting underground, the boundaries are much higher than the physical model boundaries. It is impossible to meet the geometric similarity principle. For the physical model, the boreholes are made at the centre of the model. If the distance from the borehole to the boundary is far enough for the blasting minimum resistance line, the test results will not be significantly influenced. Thus the geometric ratio of model size and field size is selected as 1:5. Thus, as the borehole diameter is 50mm in the underground excavation, the diameter of the borehole in the physical model is 10mm according to the geometric similarity.

The properties of materials used in model tests should be as similar as possible to the prototype. However, it is impossible to obtain model materials that are completely consistent with the in-situ rock mass conditions. Therefore, the condition of material similarity can only be approximately satisfied. In this research, the concrete is considered more suitable for rock blasting model test, which has been widely used in various blasting model tests. The material similarity constant is determined by the following Equation.

$$(2.4) \quad \eta = \sigma_m / \sigma_o$$

where  $\eta$  is the material similarity constant,  $\sigma_m$  is the uniaxial compressive strength for concrete,  $\sigma_o$  is the uniaxial compressive strength for rock.

The borehole and the explosive should be considered for the blasting dynamic similarity. As the diameter of the borehole, i.e. 10 mm, is much smaller than the borehole in real excavation blasting, the dynamic similarity cannot fully be implemented. The Taian explosive is used for the physical model tests while the emulsion explosive is used for the field blast. The ratio of explosive powers for the two explosives is 0.64. Considering the material similarity of the experimental model and explosive material similarity, the similarity constant of blasting power  $e$  is calculated as follows.

$$(2.5) \quad e = \frac{q_m}{q_o} = n \frac{q'_m}{q'_o} = n\sqrt{\eta}$$

The Relationship between the consumption of explosive in the model test and the actual consumption of explosive in the filed test is determined according to Equation (2.5):

$$(2.6) \quad q_m = eq_o$$

According to the analysis about and the similarity criterion, the independent variables can be expressed by the three constants as follows, and similarity criterion, the model law of dependent variables and the similarity criterion of independent variables can be expressed by these three similarity constants. Set the prototype subscript as “O” and the model subscript as “M”, then:

$$(2.6) \quad k = \frac{H_m}{H_o} \quad k = \frac{D_m}{D_o} \quad k^3 = \frac{V_m}{V_o} \quad \eta = \frac{E_m}{E_o} \quad e = \frac{q_m}{q_o}$$

Where m indicates filed tests and the o indicates the model tests.

### 3. Physical models and test results

Four kinds of cutting forms are proposed for the physical model tests. Figure 1 illustrates the four cutting forms. The black points indicate the borehole with explosive charged, while the white holes refer to the borehole without explosive.

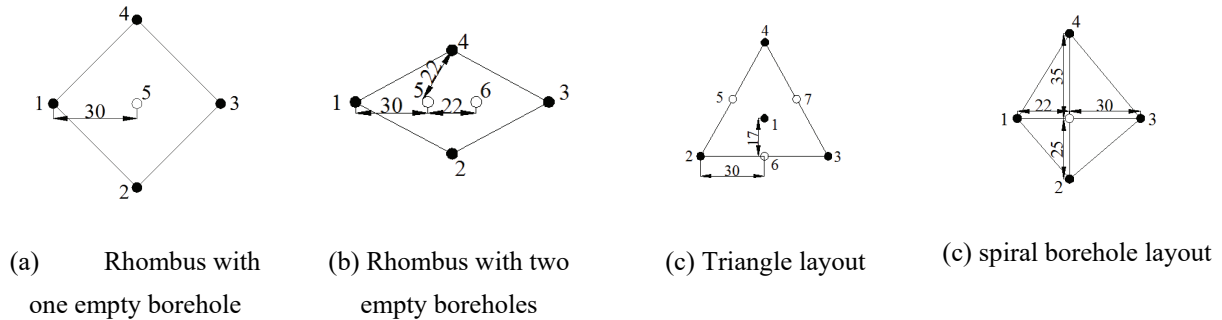


Fig. 1. Borehole layout for model tests

(Black colour indicates charged borehole while colour represents uncharged borehole)

For the test, the effect of the distance between boreholes and the layout for the charged and uncharged boreholes will be taken into account. The model material, i.e. the concrete, is made of silicate, pebbles and sands. In addition, the maximum size for pebbles should be less than 2cm, while the sand size should be less than 1mm. The ration for the silicate, pebbles, sands and water is 52/88/63/21 in terms of quantity. The boreholes of 10 mm in diameter are prefabricated in models. After 28 days, the strength of the model can meet the requirements. Figure 2 illustrates the concrete models.



Fig. 2. The concrete materials

Two types of concrete models are made as illustrated in Figure 3 for the compressive strength test and tensile strength test. The concrete parameters can be found in Table 2. The parameters for the explosives and the physical models can be found in Table 3 as follows. Four groups of the tests are taken, while each group of the tests includes two tests. Figure 4 illustrates the fracture patterns after blasting.

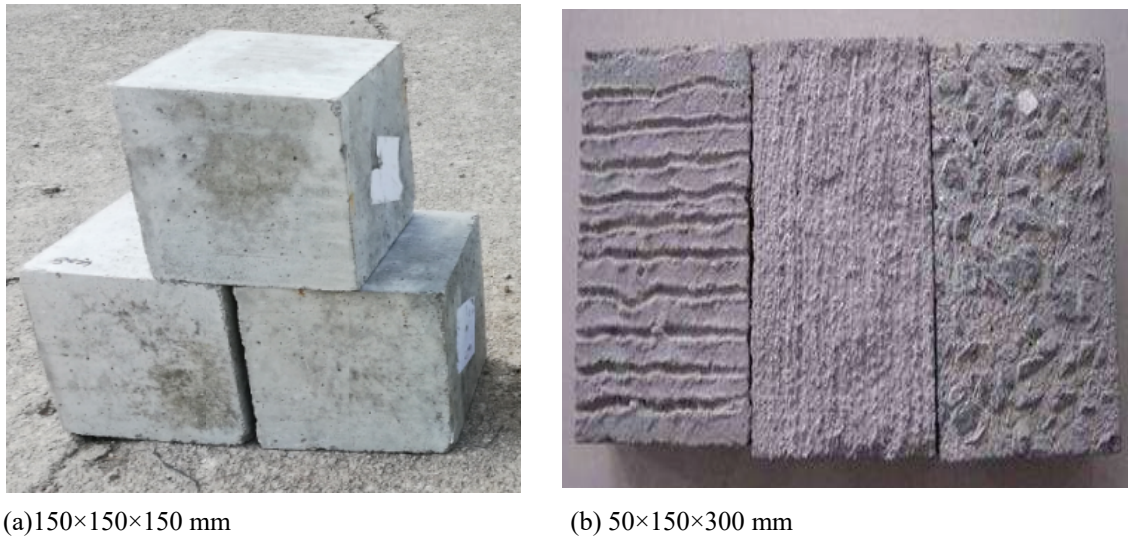


Fig. 3. The concrete samples

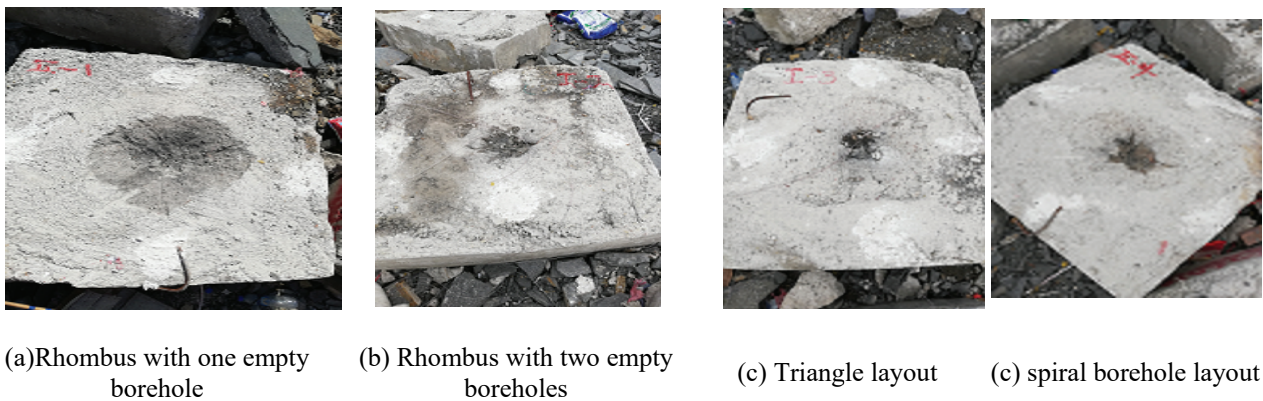


Fig. 4. The Blasting results

#### 4. Analysis of cutting blasting tests

Cutting depth, hole utilization rate, blasting volume and blasting lumpiness are important indexes to evaluate the blasting effect. After each test, the cut depth, hole utilization rate, blasting volume and blasting lumpiness are collected and shown in Table 1.

Table 1. Dimensional analysis for rock and explosive parameters

|                      | Physical Parameters  | Unit     | Symbol   | Dimension Analysis |
|----------------------|----------------------|----------|----------|--------------------|
| Dependent Variable   | Blasting footage     | m        | $H$      | $L$                |
|                      | volume               | $m^3$    | $V$      | $L^3$              |
|                      | Fragmentation        | m        | $D$      | $L$                |
| Independent Variable | Minimum Burden       | m        | $w_d$    | $L$                |
|                      | Depth of the hole    | m        | $h$      | $L$                |
|                      | Hole radius          | m        | $r_b$    | $L$                |
|                      | Radius Explosive     | m        | $r_c$    | $L$                |
|                      | Row spacing          | m        | $a$      | $L$                |
|                      | Spacing of Boreholes | m        | $b$      | $L$                |
|                      | Density of Explosive | $kg/m^3$ | $\rho_c$ | $FL^4T^2$          |
|                      | Detonation Velocity  | m/s      | $v$      | $LT^{-1}$          |
|                      | Charge Consumption   | $kg/m^3$ | $q$      | $FL^4T^2$          |
|                      | Rock Density         | $kg/m^3$ | $\rho_r$ | $FL^4T^2$          |

Figure 5 illustrates the measuring cutting depths after blasting. The cutting depths are significantly related to the utilization rate of blast hole and the cutting forms. According to figures 6 and Figure 7, for the same explosive consumption, spiral cut depth of cut blasting and the blasting hole utilization were superior to the other three straight hole cut blasting model. The blast hole utilization rate for spiral cut reached 83.0%, which increases by 16.08%, 3.11% and 1.22% compared with single diamond cut empty hole, double diamond cut empty hole and the triangular prism shape cut, respectively.

After each test, fine dry sand was filled into the plastic film above the cavity so that the fine sand was flush with the model level. The volume of the recovered fine sand measured with the measuring cylinder is the volume of the blasting body after blasting. The blasting volume is measured, as shown in Figure 8.



Fig. 5. Measuring the Cutting depths

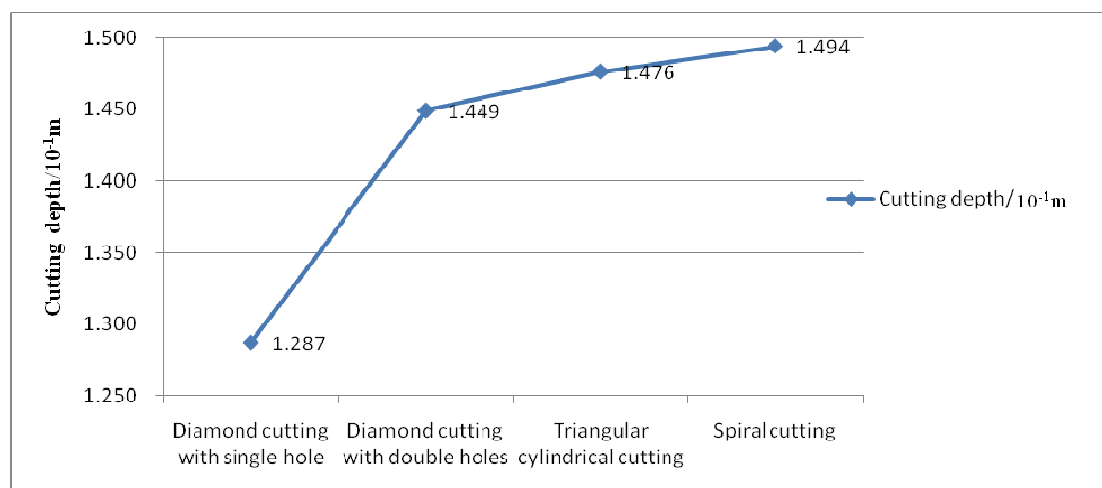


Fig. 6. The Relationship between cutting forms and cutting depths

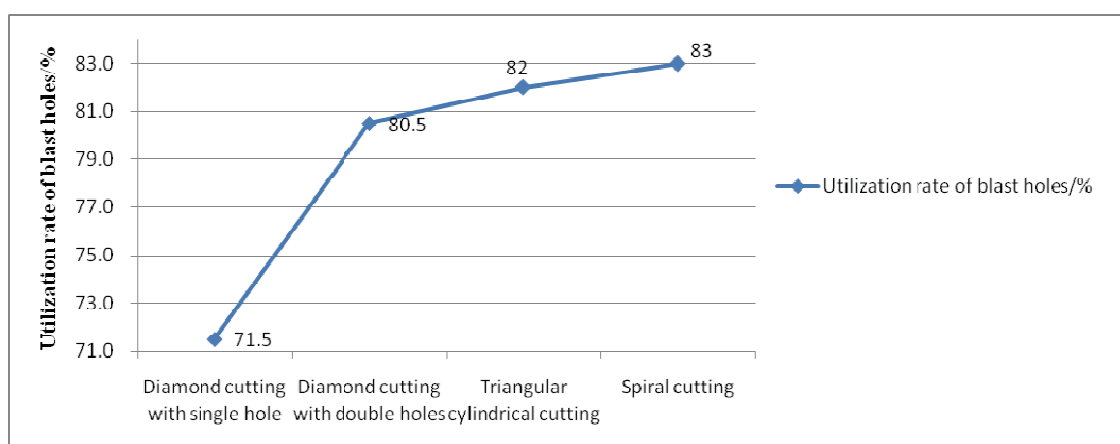


Fig. 7. The Relationship between utilization of boreholes and cutting depths

According to Figure 9, it can be seen that under the same explosive consumption, the blasting volume of spiral cutting blasting is better than that of the other three straight hole cutting blasting models in terms of blasting efficiency. The volume of the blasting body reaches  $3.915 \times 10^{-3} \text{ m}^3$ , which is 30.07%, 4.26% and 1.69% higher than that of single hole diamond cutting, double hole rhombic cutting and triangular column cutting, respectively.



Fig. 8. Measuring the blasted Volume

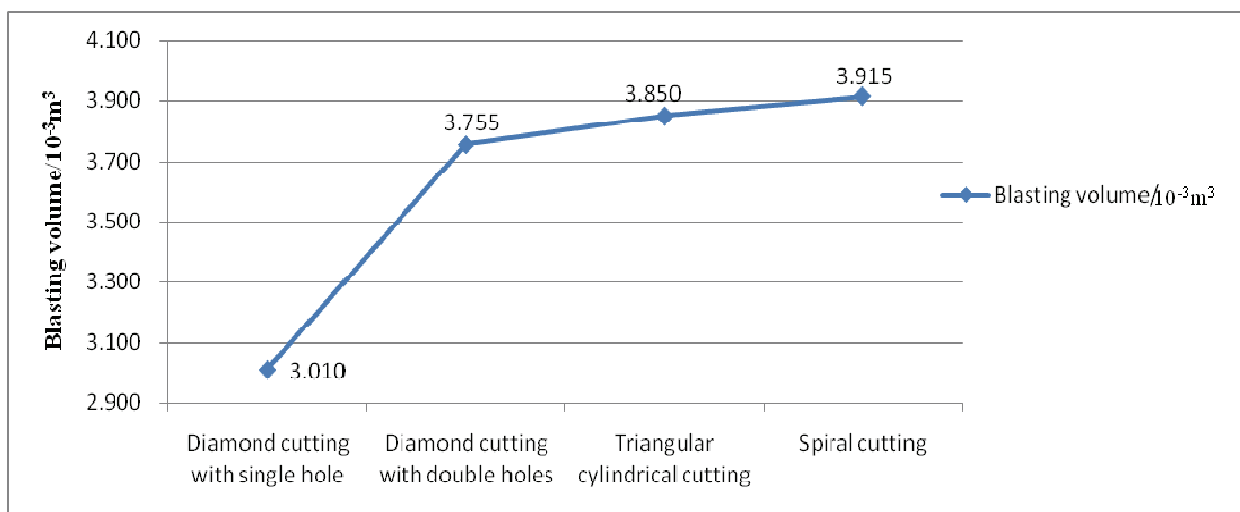


Fig. 9. The relationship between cutting forms and blasted volumes

## 5. Statistical score of model cutting blasting fragmentation

After the completion of each model blasting test, the blasting fragmentation was statistically analysed. The zbsx-92a shaker type dual-purpose vibrating pendulum screening machine and the national new standard square hole stone screen produced by Zhejiang Shangyu Xinguang instrument and equipment factory are used to screen according to a certain particle size grade, and then the weight and total weight of each grade are weighed by electronic platform scale. Figure 10, 11, 12 and Figure 13 illustrates the blasting fragmentation screening and weighing.



Fig. 10. Screening machine



Fig. 11. Fragments from four types of cutting blasts



Fig. 12. Blasting fragmentation screening

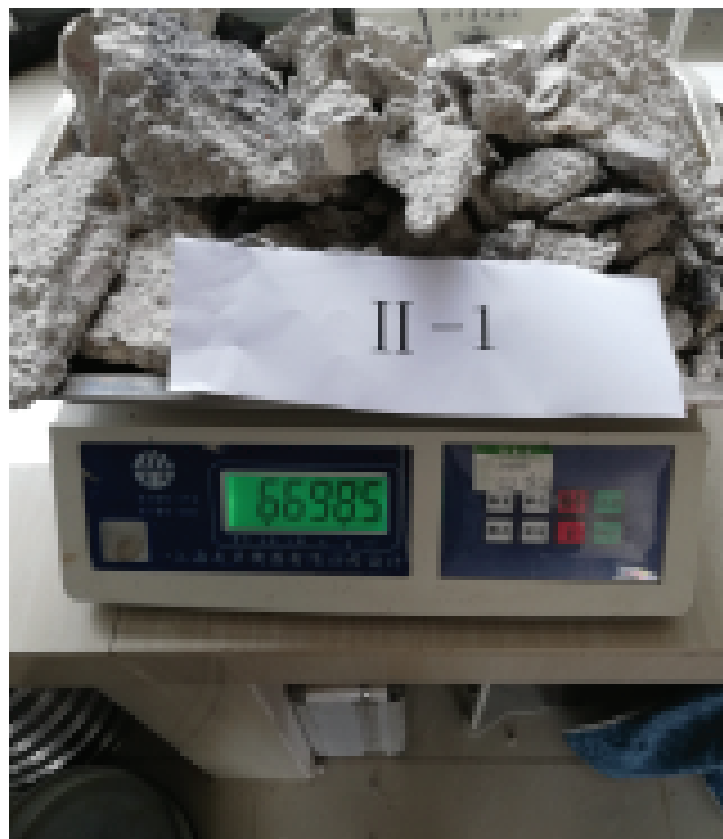


Fig. 13. Blasting fragmentation weighing

According to the blasting fragmentation distribution, the particle size can be divided into 7 grades. The blasting fragmentation distribution of each group of model tests is shown in Table 2. According

to the blasting fragmentation screening statistical in Table 2, the distribution histograms of blasting fragmentation for four different model tests are obtained, as shown in Figure 14.

Table 2. Blasting lumpiness screening statistics for different cutting forms

| Cutting Forms                    |      | Degrees/mm                    | <9.5  | 9.5~19 | 19~31.5 | 31.5~53 | 53~75  | 75~90  | >90     |
|----------------------------------|------|-------------------------------|-------|--------|---------|---------|--------|--------|---------|
| Rhombus with one empty borehole  | II-1 | Mass/kg                       | 0.225 | 0.562  | 1.089   | 1.220   | 0.716  | 1.168  | 1.719   |
|                                  |      | Total ,ass/kg                 | 0.225 | 0.787  | 1.876   | 3.096   | 3.812  | 4.980  | 6.699   |
|                                  |      | Mass percent /%               | 3.359 | 8.389  | 16.256  | 18.212  | 10.688 | 17.435 | 25.661  |
|                                  |      | Cumulative mass percentage /% | 3.359 | 11.748 | 28.004  | 46.216  | 56.904 | 74.339 | 100.000 |
| Rhombus with two empty boreholes | I-2  | Mass/kg                       | 0.276 | 0.822  | 1.358   | 1.486   | 0.680  | 1.186  | 1.451   |
|                                  |      | Total ,ass/kg                 | 0.276 | 1.098  | 2.456   | 3.942   | 4.622  | 5.808  | 7.259   |
|                                  |      | Mass percent /%               | 3.802 | 11.324 | 18.708  | 20.471  | 9.368  | 16.338 | 19.989  |
|                                  |      | Cumulative mass percentage /% | 3.802 | 15.126 | 33.834  | 54.305  | 63.673 | 80.011 | 100.000 |
| Triangle layout                  | I-3  | Mass/kg                       | 0.319 | 1.011  | 1.467   | 1.741   | 0.922  | 1.260  | 1.219   |
|                                  |      | Total ,ass/kg                 | 0.319 | 1.330  | 2.797   | 4.538   | 5.460  | 6.720  | 7.939   |
|                                  |      | Mass percent /%               | 4.018 | 12.735 | 18.478  | 21.930  | 11.614 | 15.871 | 15.354  |
|                                  |      | Cumulative mass percentage /% | 4.018 | 16.753 | 35.231  | 57.161  | 68.775 | 84.646 | 100.000 |
| spiral borehole layout           | II-4 | Mass/kg                       | 0.452 | 1.238  | 1.582   | 1.721   | 0.814  | 0.759  | 1.271   |
|                                  |      | Total ,ass/kg                 | 0.452 | 1.690  | 3.272   | 4.993   | 5.807  | 6.566  | 7.837   |
|                                  |      | Mass percent /%               | 5.768 | 15.797 | 20.186  | 21.960  | 10.386 | 9.685  | 16.218  |
|                                  |      | Cumulative mass percentage /% | 5.768 | 21.565 | 41.751  | 63.711  | 74.097 | 83.782 | 100.000 |

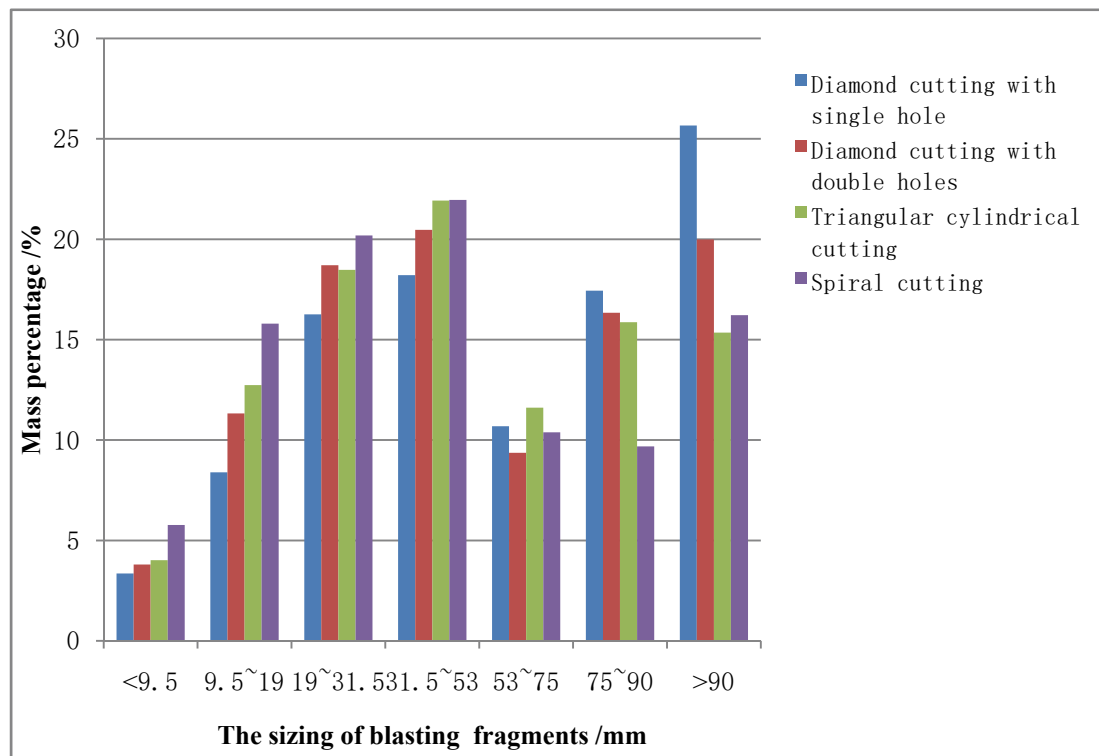


Fig. 14. Histogram of blasting fragmentation distribution of different cutting models

According to the analysis in Figure 14, for the block size < 9.5 mm, 9.5 mm ~19 mm, 19 mm ~31.5 mm and 31.5 mm ~53 mm, the four kinds of straight hole cutting model specimens contain blasting blocks, and the maximum mass percentage is spiral cutting mode, and the minimum is single hole rhombic cutting mode. In the range of 53 mm ~75 mm, the four kinds of straight hole cutting model specimens contain blasting blocks, the largest mass percentage is triangular column cutting mode, and the minimum is double empty hole rhombic cutting mode. In the range of 75 mm ~90 mm, the four kinds of straight hole cutting model specimens contain blasting blocks, and the largest mass percentage is single hole rhombic cutting mode, and the minimum is spiral cutting mode. In the range of > 90 mm, the four kinds of straight hole cutting model specimens contain blasting blocks, and the largest mass percentage is single hole rhombic cutting mode, and the minimum is triangular cylinder cutting mode.

According to statistical table 5 of blasting fragmentation screening, the relationship curve between the cumulative percentage content of each fragmentation size and the linear size of fragmentation is obtained, as shown in Figure 15–18.

By using Origin software, the cumulative percentage of block size in single hole rhombic cutting model experiment is fitted by polynomial regression, and the fourth order polynomial regression analysis expression is obtained as follows:

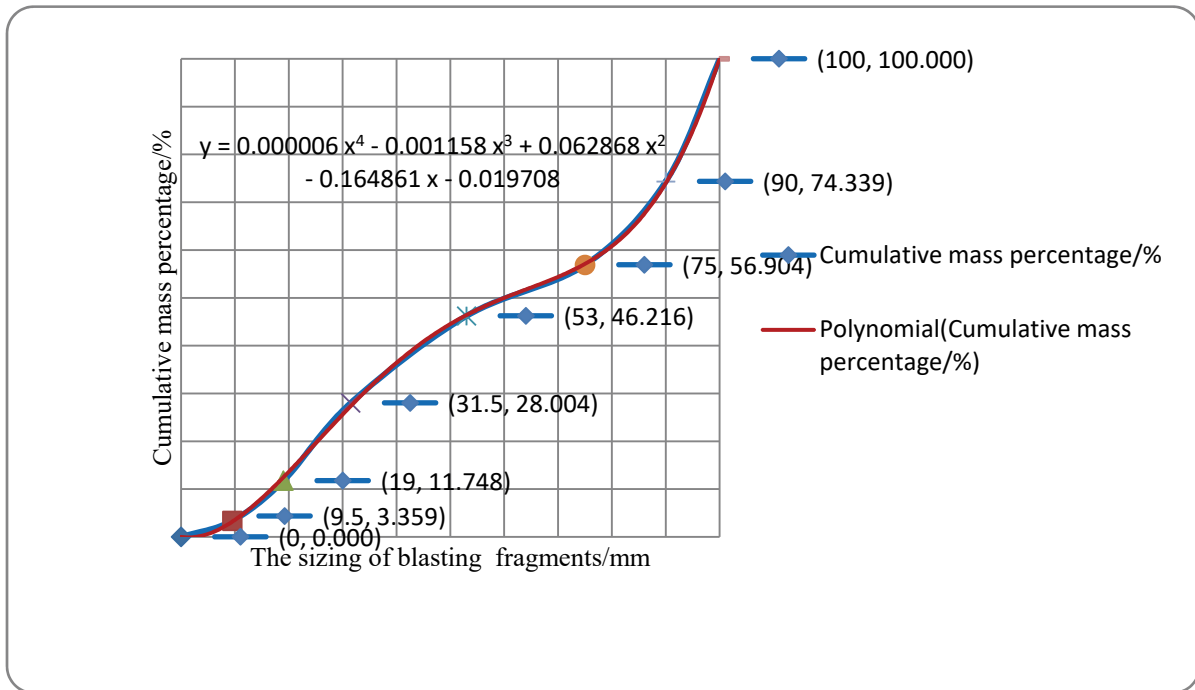


Fig. 15. Relationship between cumulative percentage of blasting fragmentation and linear size of single hole rhombic cutting model

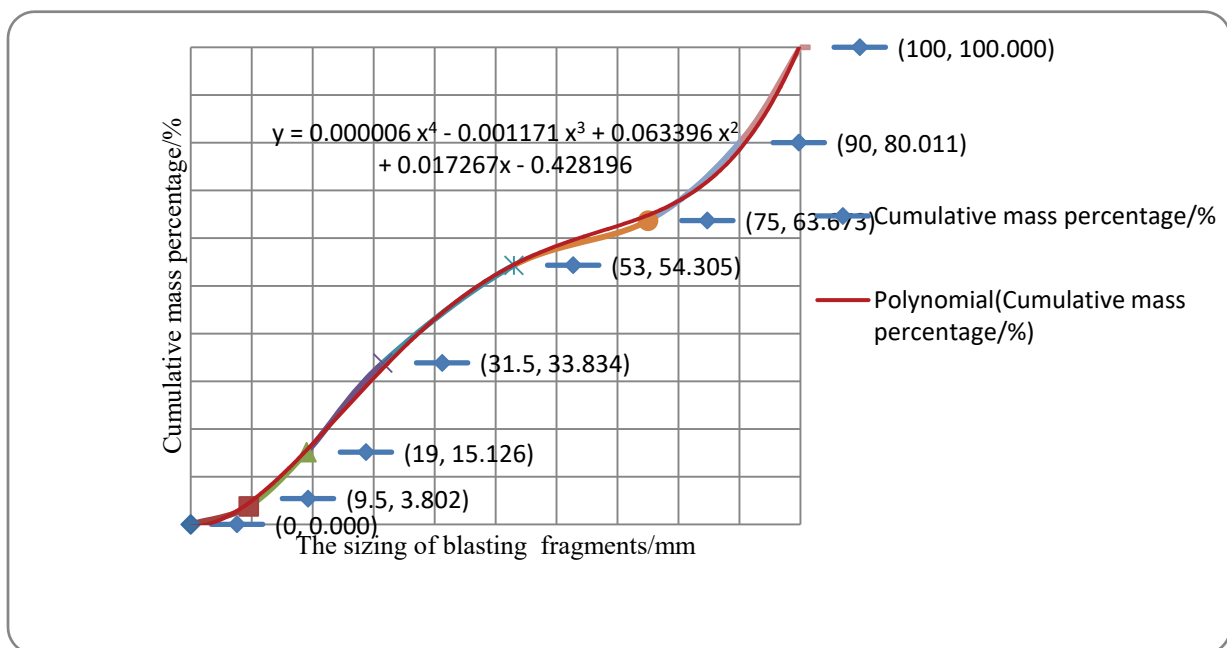


Fig. 16. Relation curve between cumulative percentage of blasting fragmentation and linear size of block size in rhombic cutting model with double empty holes

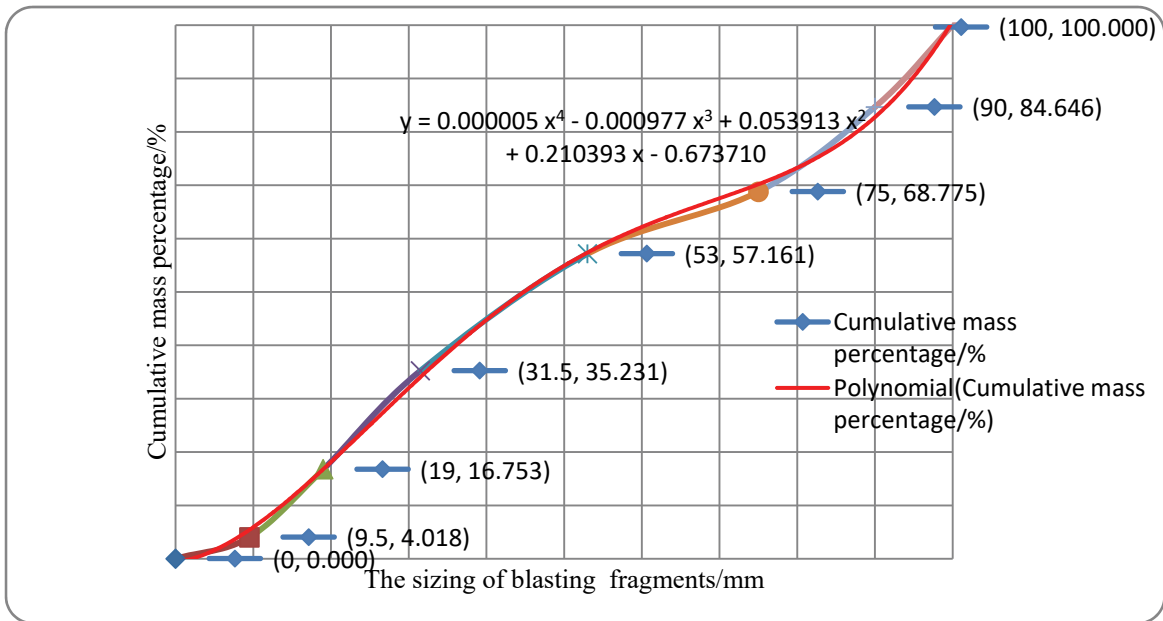


Fig. 17. Relation curve between cumulative percentage of blasting fragmentation and linear dimension of triangular cylindrical cutting model

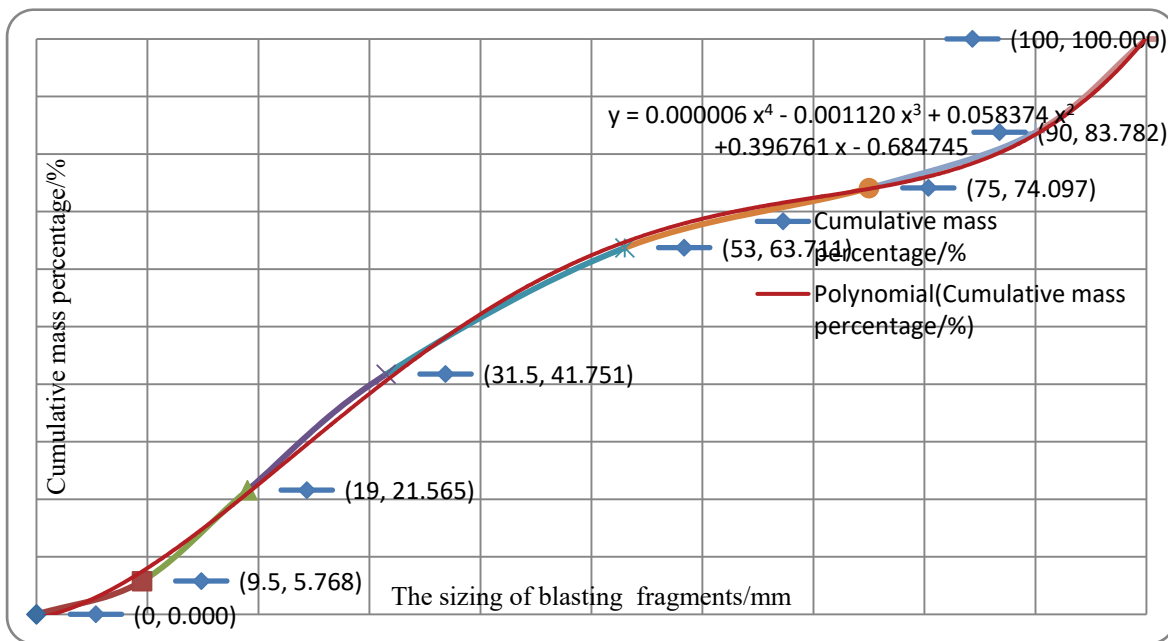


Fig. 18. Curve of Relationship between cumulative percentage of blasting fragmentation and linear size of fragmentation in spiral cutting model

$$(5.1) \quad y(x) = 0.000006x^4 - 0.001158x^3 + 0.062868x^2 - 0.164861x - 0.019708$$

The average block size of single hole rhombic cutting model experiment is 97.15 mm; if take 55 mm as the big block size, which is unqualified. The unqualified block rate can be expressed as follows.

$$(5.2) \quad \eta = 1 - y(55)$$

Thus:  $\eta = 1 - 43.33\% = 56.67\%$

According to the relationship between the cumulative percentage content and the linear size of the block size in the double hole rhombic cutting model experiment shown in Figure 16, the fourth-order polynomial regression analysis expression of the cumulative percentage content of the block size in the double empty hole rhombic cutting model experiment can be obtained as follows

$$(5.3) \quad y(x) = 0.000006x^4 - 0.001171x^3 + 0.063396x^2 + 0.017267x - 0.428196$$

Therefore, it can be calculated that the average block size is 49.91mm and the block ratio is:

$$(5.4) \quad \eta = 1 - y(55) = 1 - 52.37\% = 47.63\%$$

According to the relationship between the cumulative percentage content and the linear size of the block size in the triangular cylindrical cutting model experiment in Figure 17, the fourth-order polynomial regression analysis expression of the cumulative percentage content of the block size in the triangular cylindrical cutting model experiment can be obtained as follows.

$$(5.5) \quad y(x) = 0.000005x^4 - 0.000977x^3 + 0.053913x^2 + 0.210393x - 0.673710$$

It can be calculated that the average block size is 45.59mm and the block ratio is:

$$(5.6) \quad \eta = 1 - y(55) = 1 - 57.19\% = 42.81\%$$

According to the relationship between the cumulative percentage content of the spiral cutting model experiment and the linear size of the block size in Figure 18, the fourth-order polynomial regression analysis expression of the cumulative percentage content of the block degree in the spiral cutting model experiment can be obtained as follows:

$$(5.7) \quad y(x) = 0.000006x^4 - 0.001120x^3 + 0.058374x^2 + 0.396761x - 0.684745$$

It can be calculated that the average block size of spiral cutting model experiment is 38.20 mm, and the block ratio is:

$$(5.8) \quad \eta = 1 - \gamma(55) = 1 - 66.28\% = 33.72\%$$

To sum up, for four kinds of straight hole cutting model tests under the same explosive consumption, from the main indicators such as cutting depth after blasting, blasting hole utilization rate, blasting volume, blasting average fragmentation, blasting block rate and other main indicators, the spiral cutting hole layout mode is better than other models is obtained. Therefore, it can be concluded that in the process of tunnel excavation construction and production of underground space and connecting passage supporting project in the core section of Gui'an new area, the spiral cutting hole layout method is the optimal one-time blasting roadway forming technical scheme.

## 6. Conclusion

In this research, the relationship between cutting forms and blasting effects has been studied. Similarity theory is proposed for the experimental study of the rock blasting. Then four experimental modes with different cutting forms are used to study the blasting effect due to the cutting forms. Through the physical model test, the following conclusions can be obtained:

- The physical model test is carried out on the tunnel cross-section hole layout of the selected four cutting modes. The similarity theory is applied in the model test. The material, geometry, explosion force and other similar problems involved in the test are comprehensively analysed and studied. On the basis of meeting the similarity law and the similarity criterion, a total of 8 model tests were carried out. The test results obtained the quantitative indexes of cutting depth, hole utilization rate, blasting volume, average fragmentation and blasting block rate of four cutting modes.
- Through the comprehensive comparison and Optimization Research of the test results, it is concluded that the cutting depth, hole utilization rate, blasting volume, average blasting fragmentation and blasting block rate of spiral cutting model are better than the other three straight hole cutting models.
- The results of the model test also obtained the parameters of blast hole spacing and millisecond blasting time, which provided theoretical basis for field test.

## Acknowledgments:

This research is partly supported by the Funding for new arrival lecturers of Kunming University of Science and Technology (Grant number KKSJ201867017), Scientific research fund project of Yunnan provincial department of education (Grant No. 2020J0051), and Funding from Research Center for Analysis and Measurement KUST (Analytic and Testing Research Center of Yunnan, Grant number 2020T20180040), which are greatly appreciated.

## References

- [1] Sato, T., T. Kikuchi, and K. Sugihara, "In-situ experiments on an excavation disturbed zone induced by mechanical excavation in Neogene sedimentary rock at Tono mine, central Japan," *Engineering geology* 56(1): pp. 97–108, 2000. [https://doi.org/10.1016/S0013-7952\(99\)00136-2](https://doi.org/10.1016/S0013-7952(99)00136-2).
- [2] Cunningham, C., "Fragmentation estimations and the Kuz-Ram model-Four years on", in *Proc. 2nd Int. Symp. on Rock Fragmentation by Blasting*, 1987.
- [3] Kisslinger, C., *The generation of the primary seismic signal by a contained explosion*, DTIC Document, 1963.
- [4] Kuznetsov, V., "The mean diameter of the fragments formed by blasting rock," *Journal of Mining Science* 9(2): pp. 144–148, 1973. <https://doi.org/10.1007/BF02506177>.
- [5] Clark, L.D. and S.S. Saluja, "Blasting mechanics" *Trans. Am. Inst. Min. Engrs* 229: pp. 78–90, 1964.
- [6] Langefors, U. and B. Kihlström, "The modern technique of rock blasting" Wiley, 1978.
- [7] Porter, D.D., "Crater formation in plaster of Paris models by enclosed charges" Colorado School of Mines, 1961.
- [8] Saluja, S.S., "Mechanism of rock failure under the action of explosives", in *The 9th US Symposium on Rock Mechanics (USRMS): American Rock Mechanics Association*, 1967.
- [9] Wei, X., Z. Zhao, and J. Gu, "Numerical simulations of rock mass damage induced by underground explosion" *International Journal of Rock Mechanics and Mining Sciences* 46(7): pp. 1206–1213, 2009. <https://doi.org/10.1016/j.ijrmms.2009.02.007>.
- [10] Liu, H., D. Williams, D. Pedroso, et al., "Numerical procedure for modelling dynamic fracture of rock by blasting", in *Controlling Seismic Hazard and Sustainable Development of Deep Mines: 7th International Symposium On Rockburst and Seismicity in Mines (rasim7)*, Vol 1 and 2: Rinton Press, 2009.
- [11] Saharan, M.R. and H. Mitri, "Numerical procedure for dynamic simulation of discrete fractures due to blasting," *Rock mechanics and rock engineering* 41(5): pp. 641–670, 2008. <https://doi.org/10.1007/s00603-007-0136-9>.
- [12] Ma, G. and X. An, "Numerical simulation of blasting-induced rock fractures," *International Journal of Rock Mechanics and Mining Sciences*. 45(6): pp. 966–975, 2008. <https://doi.org/10.1016/j.ijrmms.2007.12.002>.
- [13] Wang, Z.-L., Y.-C. Li, and R. Shen, "Numerical simulation of tensile damage and blast crater in brittle rock due to underground explosion," *International Journal of Rock Mechanics and Mining Sciences*. 44(5): pp. 730–738, 2007. <https://doi.org/10.1016/j.ijrmms.2006.11.004>.
- [14] Wang, Z., Y. Li, and J. Wang, "A method for evaluating dynamic tensile damage of rock", *Engineering fracture mechanics*. 75(10): pp. 2812–2825, 2008.
- [15] Zhu, Z., B. Mohanty, and H. Xie, "Numerical investigation of blasting-induced crack initiation and propagation in rocks," *International Journal of Rock Mechanics and Mining Sciences*. 44(3): pp. 412–424, 2007.
- [16] Huang, D., X.Y. Qiu, X.Z. Shi, et al., "Experimental and Numerical Investigation of Blast-Induced Vibration for Short-Delay Cut Blasting in Underground Mining," *Shock and Vibration*. 2019: 13, 2019.
- [17] Liu, K., Q.Y. Li, C.Q. Wu, et al., "A study of cut blasting for one-step raise excavation based on numerical simulation and field blast tests" *International Journal of Rock Mechanics and Mining Sciences*, 109: pp. 91–104, 2018. <https://doi.org/10.1016/j.ijrmms.2018.06.019>.
- [18] Man, K., X.L. Liu, J. Wang, et al., "Blasting Energy Analysis of the Different Cutting Methods" *Shock and Vibration*. 2018: p. 13, 2018. <https://doi.org/10.1155/2018/9419018>.
- [19] Xie, L.X., W.B. Lu, Q.B. Zhang, et al., "Analysis of damage mechanisms and optimization of cut blasting design under high in-situ stresses" *Tunnelling and Underground Space Technology*. 66: pp. 19–33, 2017. <https://doi.org/10.1016/j.tust.2017.03.009>.

- [20] Xie, L.X., W.B. Lu, Q.B. Zhang, et al., “Damage evolution mechanisms of rock in deep tunnels induced by cut blasting”, *Tunnelling and Underground Space Technology*. 58: pp. 257–270, 2016. <https://doi.org/10.1016/j.tust.2016.06.004>.
- [21] Qu, S.J., X.B. Zheng, L.H. Fan, et al., “Numerical simulation of parallel hole cut blasting with uncharged holes” ,*Journal of University of Science and Technology Beijing* 15(3): 209–214, 2008.

Received: 2021-03-06, Revised: 2021-05-06